Journal of Materials Chemistry B

PAPER

View Article Online
View Journal | View Issue

Cite this: J. Mater. Chem. B, 2015, 3, 5455

Radiolanthanide-loaded agglomerated Fe_3O_4 nanoparticles for possible use in the treatment of arthritis: formulation, characterization and evaluation in rats

Sudipta Chakraborty,[a] K. S. Sharma,[b] A. Rajeswari,[a] K. V. Vimalnath,[a] H. D. Sarma,[c] Usha Pandey,[a] Jagannath,[d] Raghumani Singh Ningthoujam,[b] Rajesh Kumar Vatsa*[b] and Ashutosh Dash*[a]

Received 13th April 2015,
Accepted 26th May 2015

DOI: 10.1039/c5tb00677e

www.rsc.org/MaterialsB

This investigation reports the preparation of agglomerated Fe_3O_4 nanoparticles and evaluation of its utility as a viable carrier in the preparation of radiolanthanides as potential therapeutic agents for the treatment of arthritis. The material was synthesized by a chemical route and characterized by XRD, FT-IR, SEM, EDX and TEM analysis. The surface of agglomerated particle possessed ion pairs ($-O^-$:Na^+) after dispersing particles in a $NaHCO_3$ solution at pH = 7 which is conducive for radiolanthanide (*Ln = ^{90}Y, ^{153}Sm, ^{166}Ho, ^{169}Er, ^{177}Lu) loading by replacement of Na^+ ions with tripositive radiolanthanide ions. Radiolanthanide-loaded particulates exhibited excellent *in vitro* stability up to ~3 half-lives of the respective lanthanide radionuclides when stored in normal saline at 37 °C. The radiochemical purities of the loaded particulates were found to be retained to the extent of >70% after 48 h of storage when challenged by a strong chelator DTPA present at a concentration as high as 5 mM, indicating fairly strong chemical association of lanthanides with agglomerated Fe_3O_4 nanoparticles. Biodistribution studies of ^{90}Y and ^{166}Ho-loaded particulates carried out after intra-articular injection into one of the knee joints of a normal Wistar rat revealed near-complete retention of the radioactive preparations (>98% of the administered radioactivity) within the joint cavity even after 72 h post injection. This was further confirmed by sequential whole-body radio-luminescence imaging. These experimental results are indicative of the potential use of radiolanthanide-loaded agglomerated Fe_3O_4 nanoparticles for the treatment of arthritis.

Introduction

Arthritis is one of the most common forms of slowly progressive, systemic, autoimmune inflammatory disorders of synovial joints which affect ~2% of adult population worldwide.[1–4] This progressive degenerative disease is characterized by uncontrolled proliferation of tissues in the inner layer of the synovial membrane leading to chronic joint inflammation.[1,3,4] This in turn leads to restricted joint mobility and partial disability and thereby severely affects the quality of life of the affected population. If synovial inflammation is left untreated, it can even lead to loss of cartilage, erosion and weakening of bones. The treatment strategy involves ablation of diseased synovial membranes followed by the regeneration of the disease-free synovium which eventually results in the reduction of inflammation in the joints, alleviation of the pain, improvement in mobility and preservation of joint functions.[1] Ablation of the synovium can be accomplished through a number of surgical and non-surgical procedures including laser surgery, use of chemicals such as osmic acid rifampicin, and use of ionizing radiation by intra-articular administration of β^- emitting radionuclides in a suitable chemical formulation. Among all these treatment modalities in practice, intra-articular administration of β^- emitting radionuclides in the form of a colloidal formulation or radiolabeled particulate (preferably of 1–10 μm size range) into the articular cavity, referred to as 'radiation synovectomy (RSV)' or 'radiosynoviorthesis', has emerged as one of the most effective option having satisfactory clinical efficacy and minimum side-effects.[2–9]

While a myriad of factors contribute to the utility of RSV, selection of an appropriate β^- emitting radionuclide of optimum tissue penetration range along with desirable radioactive decay

[a] Isotope Production and Applications Division, Bhabha Atomic Research Centre, Trombay, Mumbai 400 085, India. E-mail: adash@barc.gov.in; Fax: +91-22-25505151
[b] Chemistry Division, Bhabha Atomic Research Centre, Trombay, Mumbai 400 085, India. E-mail: rkvatsa@barc.gov.in
[c] Radiation Biology and Health Sciences Division, Bhabha Atomic Research Centre, Trombay, Mumbai 400 085, India
[d] Technical Physics Division, Bhabha Atomic Research Centre, Trombay, Mumbai 400 085, India

Table 1 Lanthanide radionuclides proposed for radiation synovectomy[2,16,19,20,23,24]

Radionuclide	Half-life	$E_{\beta(max)}$ (MeV)	Max. tissue penetration (mm)	E_γ (keV) (% ab)	Production route	σ_{th} (barns)
^{90}Y	64.1 h	2.28	11.3	—	^{89}Y(n,γ) ^{89}Y/^{90}Y Gen.	1.28
^{166}Ho	26.9 h	1.85	8.7	80.6 (6.4)	^{165}Ho(n,γ)	61.2
^{165}Dy	2.35 h	1.29	5.6	94.7 (3.6)	^{164}Dy(n,γ)	1040
^{153}Sm	46.9 h	0.81	3.5	103.0 (28.0)	^{152}Sm(n,γ)	206
^{177}Lu	6.65 d	0.497	2.0	113.0 (6.4), 208.0 (11.0)	^{176}Lu(n,γ) ^{176}Yb(n,γ,β$^-$)	2090 2.85
^{175}Yb	4.18 d	0.48	2.0	282.0 (3.1), 396.0 (6.5)	^{174}Yb(n,γ)	69
^{169}Er	9.39 d	0.34	1.0	110.9 (0.0014)	^{168}Er(n,γ)	1.95

characteristics is a key determinant that underpins its success. The β$^-$ radiation energy should be sufficient to penetrate and ablate the proliferating layer of the inflamed synovium with minimum radiation induced damaged to the underlying articular cartilage or adjacent bone underneath.[5,10–12] The radionuclide should have a half-life adequate to deliver cytotoxic radiation doses to the synovium and at the same time should be substantially less than the retention time of the radiolabeled formulation in the joint to be treated. Among the various radionuclides used for RSV, the lanthanide radionuclides such as ^{90}Y (yttrium is considered as a pseudo-lanthanide), ^{153}Sm, ^{165}Dy, ^{166}Ho, ^{169}Er, ^{175}Yb and ^{177}Lu (Table 1) have dominated the field significantly and have been profusely explored for the development of a broad panoply of radiolabeled particles/colloids/macroaggregates.[2,11–24] This is principally due to the availability of a wide variety of therapeutically useful β$^-$ emitting radionuclides among lanthanide elements having a wide range of energy (0.34–2.28 MeV). As the thickness of the proliferating membrane varies in different joints, treatment of the diseased synovium in joints of disparate size requires radionuclides of different β$^-$ particle energies. In this premise, the scope of using a single carrier platform loaded with different lanthanide radionuclides resulting in a series of radiolanthanide-loaded particulates of same material would be an interesting proposition. This is expected to pave the way for the treatment of arthritis of human joints of different sizes from finger joints than for a knee, for example, by selecting particulates loaded with the suitable lanthanide radionuclide. In pursuit of such a strategy, the possibility of using ^{90}Y, ^{153}Sm, ^{166}Ho, ^{169}Er and ^{177}Lu seemed attractive as they offer the prospect of designing radiolabeled particles with a wide spectrum of β$^-$ particle energies.

In the quest of an innovative and more effective carrier platform to deliver cytotoxic doses of radiolanthanides to the diseased synovium, our attention was turned toward use of nanomaterials as they provided unprecedented opportunities to design and synthesise novel materials which preferentially target proliferating cells in biological systems.[25,26] While the usefulness of iron oxide nanoparticles as the platform to deliver imaging probes including radionuclides and therapeutic drugs[27–32] and in hyperthermia therapy[27,33–35] have been copiously exploited, the potential utility of this substrate in the preparation of RSV agents has not yet been explored. Based on these successful propositions of iron oxide nanoparticles in medical use and given the excellent biocompatibility of Fe_3O_4, it is envisaged to use agglomerated Fe_3O_4 nanoparticles (Agl-MNP) of 1–10 μm size range as the carrier platform for developing potential radiotherapeutic agents for treatment of arthritis. The ability of magnetic Fe_3O_4 nanoparticles to absorb different elements has been utilized in recent studies on intrinsic or chelator free formulation of different radiolabeled Fe_3O_4 nanoparticles as probes for positron emission topography (PET) imaging.[32,36]

In the present study, we have adopted a similar strategy in synthesizing radiolanthanide loaded Agl-MNP. The agglomerated nanoparticles can have pores as well as –OH groups over the surface which leads to generation of surface negative charges when these particles are dispersed in neutral to alkaline pH. This would be useful for loading many metal cations on Agl-MNP including lanthanide ions. Working towards this, we describe herein the synthesis, and radiochemical and physicochemical characterization of Agl-MNPs loaded with lanthanide radionuclides namely ^{90}Y, ^{166}Ho, ^{153}Sm, ^{177}Lu and ^{169} Er for their possible utilization in the treatment of arthritis of different joints of the human body. The biological properties of ^{90}Y- and ^{166}Ho-loaded particulates were evaluated after intra-articular administration into the knee joint of Wistar rats. An optimized formulation strategy of radiolanthanide-loaded Agl-MNPs possessing adequate *in vitro* and *in vivo* stability has been the propitious outcome. To our knowledge, this is the first example where the unique physical and chemical properties associated with a nanomaterial-based carrier platform have been exploited in the preparation of radiotherapeutic agents for RSV.

Experimental

Materials and equipment

Radionuclides used in the present study were produced by a radiative neutron capture (n,γ) route in a research reactor. Spectroscopic grades (>99.99% pure) of yttrium oxide (Y_2O_3) and holmium oxide (Ho_2O_3) used as the targets for the production of ^{90}Y and ^{166}Ho, respectively, were procured from American Potash, USA. These are naturally mononuclidic in ^{89}Y and ^{165}Ho. For the production of ^{153}Sm, ^{169}Er and ^{177}Lu, isotopically enriched Sm_2O_3 (99.8% in ^{152}Sm), Er_2O_3 (98.6% in ^{168}Er) and Lu_2O_3 (82% in ^{176}Lu) (all >99.99% pure) were used as the target materials. These were all procured from Trace Science International, Canada. No-carrier-added (NCA) ^{90}Y was obtained from a ^{90}Sr/^{90}Y generator system based on an electrochemical separation technique developed in-house.[37] Ferric chloride ($FeCl_3.6H_2O$), ferrous sulphate ($FeSO_4{\cdot}7H_2O$), suprapure HCl and de-ionized water

(resistivity higher than 18.2 MΩ cm) were procured from Merck, Darmstadt, Germany. All other chemicals used in the experiments were of AR grade and procured from Aldrich Chemical Company, USA.

The radiochemical processing of irradiated targets was performed in a 100 mm lead shielded glove box with remote handling provisions maintained under aseptic conditions. The radioactivity assay of all the radionuclides except ^{90}Y was carried out by high resolution gamma ray spectrometry using an HPGe detector (EGG Ortec/Canberra detector) coupled to a 4000 multichannel analyzer (MCA) system. Energy and efficiency calibration of the HPGe–MCA system was carried out using ^{152}Eu and ^{133}Ba reference sources obtained from Amersham, USA. The assay of gamma emitting radionuclidic impurities present in the radionuclides produced, if any, was also carried out using the same system. The radioactivity of ^{90}Y was measured using a liquid scintillation counter (Tri-Carb 3100TR Liquid Scintillation analyzer, Perkin Elmer, USA), calibrated for the assay of ^{90}Y. In the case of ^{90}Y, the assay of Sr radionuclides present was carried out by the extraction paper chromatography (EPC) technique.[38] Measurements of ^{90}Y and $^{89/90}$Sr activities during EPC studies were performed using a liquid scintillation counter. All other radioactivity measurements were performed using a well type NaI(Tl) scintillation counter (Mucha, Raytest, Germany).

Xylazine hydrochloride and ketamine hydrochloride used for anaesthetizing the animals during animal were procured from local suppliers. Bioluminiscence images of the animals after administration of the radiolabeled preparation were recorded using a Photon Imager (Biospace Lab, France). All the animal experiments were conducted in strict compliance of the relevant national laws relating to the conduct of animal experiments in India.

Synthesis of agglomerated Fe_3O_4 nanoparticles (Agl-MNP)

Aqueous solutions of ferric chloride (0.1 M, 20 mL) and ferrous sulphate (0.1 M, 10 mL) were mixed by stirring. The resultant solution was made alkaline by addition of 20 mL of 0.2 M NaOH. The black precipitate formed was separated using a magnet, washed five times with water and dried after stirring for 1 hour. The precipitate was further dried using acetone. Subsequently, 1 g of Fe_3O_4 obtained was treated with 10 mL of 0.1 M $NaHCO_3$. This process leads to the formation of highly agglomerated nanoparticles of Fe_3O_4, which gradually settles in aqueous medium.

Physicochemical characterization

The prepared samples of Agl-MNP were characterized using X-ray diffractometry (using a Rigaku Miniflex 600 X-ray diffractometer) and the crystallite size (t) was calculated using the Scherrer equation $t = (0.9\lambda)/(B\cos\theta)$, where λ is the wavelength of Cu Kα, B the half width at maximum intensity and θ the Bragg's angle. The surface functionalization of Fe_3O_4 particles was characterized using a Fourier Transform Infrared (FT-IR) Spectrometer (Bomem FTIR). TEM images of the particles were recorded using a transmission electron microscope (2000 FX, JEOL, Japan). X-ray photoelectron spectra (XPS) were recorded in a UHV chamber (base pressure $< 2 \times 10^{-8}$ mbar) using a VG CLAM-2 analyzer with a non-monochromatic twin Mg X-ray ($h\nu \sim 1253.6$ eV) source. All binding energies were referenced to the C 1s peak at 284.6 eV.

Production and quality control of radionuclides

A measured quantity (few mg) of natural Y_2O_3 (100% ^{89}Y), Ho_2O_3 (100% ^{165}Ho), enriched Sm_2O_3 (99.8% in ^{152}Sm) and Er_2O_3 (98.6% in ^{168}Er) targets were weighed separately into clean quartz ampoules which were subsequently flame sealed. The sealed ampoule was put inside a standard aluminum container, sealed and irradiated in DHRUVA research reactor at Bhabha Atomic Research Centre, India, at a thermal neutron flux of $\sim 1 \times 10^{14}$ neutrons per cm^2 per second (n cm^{-2} s^{-1}). The durations of irradiation were 7 d (for Ho_2O_3 and Sm_2O_3), 14 d (for Y_2O_3) and 28 d for Er_2O_3. In the case of Lu_2O_3, a stock solution of lutetium target (85.5% in ^{176}Lu) was prepared by dissolving enriched Lu_2O_3 powder in 0.01 M suprapure HCl to obtain 2 mg mL^{-1} Lu concentration. A measured aliquot of this solution (typically 0.1 mL) was dispensed in a quartz ampoule and carefully evaporated to dryness. The ampoule was subsequently flame sealed, encapsulated in an Al container and irradiated in a DHRUVA reactor at a thermal neutron flux of $\sim 1 \times 10^{14}$ n cm^{-2} s^{-1} for a duration of 21 d. Following neutron irradiation, the targets were retrieved from the quartz ampoules and dissolved in 0.1 M suprapure HCl (0.01 M suprapure HCl, in the case of Lu target) by heating under reflux for a period of 15 min in a sterile round bottom flask. The resultant solution was evaporated to near dryness, cooled and reconstituted in 5 mL of deionized water. NCA ^{90}Y was obtained from an ^{90}Sr/^{90}Y generator system developed in-house.[37] Y-90 is obtained as $^{90}YCl_3$ solution in 0.1 N HCl from this generator following the procedure reported earlier,[37] which was subsequently used.

The total activity of all the radionuclides produced was individually assayed using gamma ray spectrometry using a HPGe detector coupled to a 4K-MCA system, except that of ^{90}Y. Energy and efficiency calibration of the detector was carried out using standard ^{152}Eu and ^{133}Ba sources of the same geometry as the test samples. Prominent photo peak per second of the radionuclides (Table 1) was used for measurements of the radioactivity content. The activity of ^{90}Y produced was determined using a pre-calibrated liquid scintillation counter. For the determination of radionuclidic purity, the trace levels of co-produced gamma emitting radionuclide impurities were assayed by recording the gamma ray spectra of the sample aliquot from the batch processed, initially having high radioactive concentration, after complete decay ($8–10T_{1/2}$) of principle radionuclides in all the cases. In the case of ^{90}Y while gamma ray spectrometry was used to assay any gamma emitting radionuclidic impurity, probable impurities emitting only β^- (^{89}Sr for reactor produced ^{90}Y and ^{90}Sr in the case of NCA ^{90}Y) were assayed by the extraction paper chromatography (EPC) technique.[38] The procedure is based on the selective retention of ^{90}Y by bis(2-ethyl hexyl)phosphonic acid. In brief, 10 μL of the reagent was impregnated at a distance of 2 cm from one end of a Whatman 3 mm chromatography paper (12 × 1 cm) upon which 5 μL of ^{90}Y solution (37 MBq mL^{-1}) was

applied. The paper was dried and developed in 0.9% saline. Subsequently, the activity in each 1 cm segment of the paper was counted using a liquid scintillation counter. Under these conditions, any $^{89/90}$Sr impurity, if present, migrates to the solvent front (R_f = 0.9–1.0), while ^{90}Y remains at the point of application (R_f = 0). The counts obtained at the solvent front were then compared with the total spotted activity to determine the $^{89/90}$Sr content in the ^{90}Y sample.

Optimization of the protocol for formulation of radiolanthanide-loaded Agl-MNPs

Loading of agglomerated Fe_3O_4 magnetic nanoparticles (Agl-MNP) with ^{90}Y (reactor produced and NCA), ^{153}Sm ^{166}Ho, ^{169}Er and ^{177}Lu was achieved by mixing the radioactivity in the form of *$LnCl_3$ (Ln = Y, Sm, Ho, Er and Lu) solution (~185 MBq for ^{90}Y, ^{153}Sm ^{166}Ho and ^{177}Lu; ~37 MBq for ^{169}Er) with a suspension of particles in 0.1 M $NaHCO_3$ solution such that the pH of the reaction medium was ~8 after addition of *$LnCl_3$ solution. The mixture was kept under constant stirring at room temperature. Subsequently, the suspended particulates were allowed to settle at the bottom of the reaction tube and the supernatant was carefully separated. The *Ln-loaded particles thus obtained were subjected to a further washing using 1 mL of sterile 0.9% saline to ensure the removal of unlabeled [*Ln^{3+}] activity, if any. Finally, the radiolanthanide-loaded particulates were suspended in sterile 0.9% and autoclaved.

Several experiments were carried out by varying the reaction parameters such as concentration of particles, pH of the reaction mixture and mixing time *etc.* in order to obtain the optimized protocol for maximum yield of radiolabeled particles. In a reaction volume of 1 mL, the amount of particles was varied between 1 mg and 10 mg and the radiolabeling yield was determined in each case. The effect of variation of pH on the radiolabeling yield at room temperature was studied by adjusting the pH of the reaction mixture from 2 to 10 using either 1 M HCl or 1 M NaOH solution. The mixing time required to obtain maximum labeling yield was optimized by carrying out reactions for different time periods (0, 10, 20, 30, 60 and 120 min) at room temperature and determining the yield in each case.

Determination of yield and radiochemical purity

The loading yields of radiolanthanides on Agl-MNP were determined in the following way. An aliquot (typically, 20 μL) was withdrawn from the supernatant solution of the reaction mixture after the precipitation of Agl-MNP and the radioactivity was measured. The same aliquot was withdrawn from 'blank' (solution having identical composition to the *Ln–Agl-MNP reaction mixture without particles) and the activity was measured. The percentage radiochemical yield was determined from the activity data using the following formula:

$$\text{Percent radiolabeling yield} = \left(100 - \frac{R}{B}\right)$$

where B and R are the background-corrected *Ln activities associated with the aliquots withdrawn from the blank and supernatant solution of the reaction mixture, respectively. The radiochemical purity of the radiolabeled preparation was determined using the same technique subsequent to the removal of unlabeled *Ln activity by washing of loaded Agl-MNP using normal saline.

In vitro stability studies

The *in vitro* stability of radio-lanthanide loaded Agl-MNPs was studied in normal saline. For this, loaded particles were suspended in 1 mL of normal saline. The suspensions were stored at 37 °C up to 3 half-lives of the individual radionuclide. The radiochemical purities of the suspended *Ln–Agl-MNPs were determined at the end of different time intervals by following the technique described previously. The *in vitro* stability of the radiolabeled particulates was also ascertained by DTPA challenge (DTPA = diethylene triamine pentaacetic acid). For this, the radiolabeled formulation was suspended in 1 mL of 5 mM aqueous solution of DTPA (pH ~ 6.5) and the mixture was stored at room temperature. The percentage radiochemical purity *Ln–Agl-MNPs in the presence of strong chelator DTPA was determined at regular time intervals up to 48 h of storage following the same technique as described above.

Synthesis of cold Y/Ho–Agl-MNPs

Agl-MNP (50 mg) was suspended in 4 mL of 0.1 M $NaHCO_3$ solution. To this suspension, 1 mL of YCl_3/$HoCl_3$ solution in 0.01 M suprapure HCl containing 50 mg of yttrium/holmium was added and it was mixed thoroughly at room temperature for 24 h using a magnetic stirrer. The pH of the mixture was found to be ~7–8. Subsequently, the mixture was centrifuged and the supernatant was removed carefully. The precipitated Y/Ho-loaded particles were washed thrice with de-ionized water and dried under an IR lamp. Subsequently, these particulates were analysed by SEM and EDX techniques.

SEM and EDX analyses

The surface morphology and particle size distribution of Y/Ho-loaded Agl-MNPs were examined using SEM (AIS2100 SERON Technologies, South Korea). For SEM analysis powder samples were spread over a mirror polished Si substrate using acetone, dried and tapped to remove any loose particles prior to loading into the SEM chamber. All the micrographs were recorded at the same magnification so as to compare the size and shape of samples. Elemental analyses were carried out using the same samples by the EDX technique.

In vivo studies in an animal model

The pre-clinical biological evaluation of ^{90}Y- and ^{166}Ho-loaded Agl-MNPs was done by carrying out bio-distribution and radio-luminescence imaging studies in normal Wistar rats. The radio-luminescence imaging (also known as Cerenkov luminescence imaging) technique is based on the emission of visible light during the passage of particulate radiation from the decay of certain radionuclides thorough the condensed phase (that of biological tissue in the present case).[39] For biodistribution studies, loaded particles (~2 MBq) suspended in 100 μL of normal saline were injected intra-articularly into one of the knee joints of each animal. For intra-arterial administration,

the rats were first anaesthetized using a combination of xylazine hydrochloride and ketamine hydrochloride. Subsequently, the left knee area of the animals was clipped and prepared aseptically. The knee joint was approached craniolaterally in between *lig. collaterale laterale genus* and *m. gastrocnemius lateralis*, below *condulis lateralis osis femoris* and the radiolabeled particulates were administered. ^{90}Y-loaded Agl-MNP was synthesized using ^{90}Y produced by the (n,γ) route. Normal saline (100 μL) was injected into the other joint (control). The animals administered with ^{90}Y-Agl-MNP were sacrificed by CO_2 asphyxiation at the end of 3, 24 and 72 h post-injection (p.i.). On the other hand, animals administered with ^{166}Ho-MNPs were sacrificed at 3, 24 and 48 h p.i. (p. i. = post injection) time points. Four rats were used for each time point. Major organs and tissues were excised, washed with saline (except blood), dried, weighed and the activity associated with each of them was measured in a flat-type NaI(Tl) scintillation counter. The distribution of the activity in different organs was calculated as the percentage of injected activity (dose) (%ID) per organ and percentage of injected activity per gram of the organ (%ID per g) from these data. The activity accumulated per gram of femur was considered for obtaining the total skeletal uptake assuming the skeletal weight to be 10% of the total body weight.[21,22] The total uptake in blood, skeleton and muscle were calculated by considering that the respective tissues constitute 7%, 10% and 40% of the total body weight.[21,22] The percentage of activity excreted is indirectly ascertained by subtracting the activity accounted in all the organs from the total injected activity. For radio-luminescence imaging, ^{90}Y- and ^{166}Ho–Agl-MNP preparations (~10 MBq) suspended in 100 μL of normal saline were injected into the joints. Prior to the acquisition of images, the animals were anesthetized using a combination of xylazine hydrochloride and ketamine hydrochloride. Sequential whole-body radio-luminescence images were acquired in a Photon Imager at the same time points p.i. when the bio-distribution studies were carried out.

All animal experiments were performed in compliance with the relevant laws and institutional guidelines of the Bhabha Atomic Research Centre, and also state that the institutional Animal Ethics Committee has approved the experiments.

Results

The primary objective of this investigation aims at developing a synthetic route for the large scale preparation of agglomerated Fe_3O_4 nanoparticles, structural characterization of the material, and evaluation of their usefulness as a viable carrier platform for the preparation of radiolanthanide-loaded particles for use in RSV. With a view to accomplish the desired goal, a systematic approach was pursued.

Synthesis and characterization of agglomerated Fe_3O_4 nanoparticles

The schematic diagram for formation of agglomerated Fe_3O_4 nanoparticles is shown in Fig. 1. The adopted synthetic protocol led to the formation of agglomerated nanoparticles with a size (1–10 μm agglomerated size) optimal for retention within the joint cavity without extra-articular leakage to other healthy organs. Moreover, the protocol enables cost-effective preparation of agglomerated Fe_3O_4 nanoparticles in large quantities with high reproducibility with only minor batch-to-batch variations in yield.

The X-ray diffraction (XRD) pattern shows a cubic structure of Fe_3O_4 with lattice parameter a = 8.38 Å (Fig. 2(i)), which is matching with the reported value.[40] Fourier transform infrared (FTIR) spectra of Fe_3O_4 particles before and after treatment with $NaHCO_3$ suggest that both have a characteristic Fe–O peak at 600 cm^{-1} (Fig. 2(ii)).[41] Additionally, surface –OH groups on the Fe_3O_4 particles were identified by characteristic peaks at 3400 (stretching) and 1650 cm^{-1} (bending).[40,41] However, after treatment of the $NaHCO_3$ solution, the IR spectrum does not show the peak at 3400 cm^{-1}. This observation is probably attributed to the formation of O^-:Na^+ ion-pairs on the surface of the particles. This will lead to negative surface charges on the particles and expected separation of the particles. However, magnetic dipole–dipole interaction might have dominated over electrostatic separation force resulting in the agglomeration of smaller crystallites. The peak at 1640 cm^{-1} will be related to the carbonate residue from the $NaHCO_3$ solution. The TEM image of Fe_3O_4 particles shows the highly agglomerated particles (Fig. 2(iii)) and its selected area electron diffraction (SAED) pattern (Fig. 2(iv)) suggests the highly crystalline phase with the cubic structure.

Since the XRD pattern of Fe_3O_4 is similar to that of γ-Fe_2O_3, it is difficult to say whether compound is Fe_3O_4 or γ-Fe_2O_3. In order to identify the compound, we have carried out XPS experiments of the sample. Fig. 3(a) and (b) show the XPS spectra of Fe 2p and O 1s. The position of the Fe $2p_{3/2}$ peak is found to be at 709 eV. There is a very weak satellite peak at ~719 eV. In the literature, Fe $2p_{3/2}$ peak positions in Fe_3O_4 and γ-Fe_2O_3 were 709 and 711 eV, respectively, and also γ-Fe_2O_3 has an extra peak (known as satellite) at 719 eV.[42] It is concluded that our prepared compound is Fe_3O_4. The position of the O 1s peak is found at 530 eV, which is similar to the reported one.[42] However, there is an asymmetric nature in the peak at a higher binding energy side. This suggests that oxygen stoichiometry is not maintained. This is due to inhomogeneity of oxygen at the core as well as surface of nanoparticles.

Production and quality control of the radionuclides

The specific activity and radionuclidic purity of the radionuclides produced in the reactor at 6 h after the end of irradiation (EOI) are shown in Table 2. Apart from the reactor-produced radionuclides, NCA ^{90}Y was separated from ^{90}Sr/^{90}Y following the electrochemical separation technique as described in the experimental section. It is evident from Table 2 that all the radionuclides under consideration were produced with a very high radionuclidic purity of >99.9% and hence suitable for clinical utilization. Depending upon the cross section of radiative neutron capture of the corresponding target nuclide, the specific activities of the

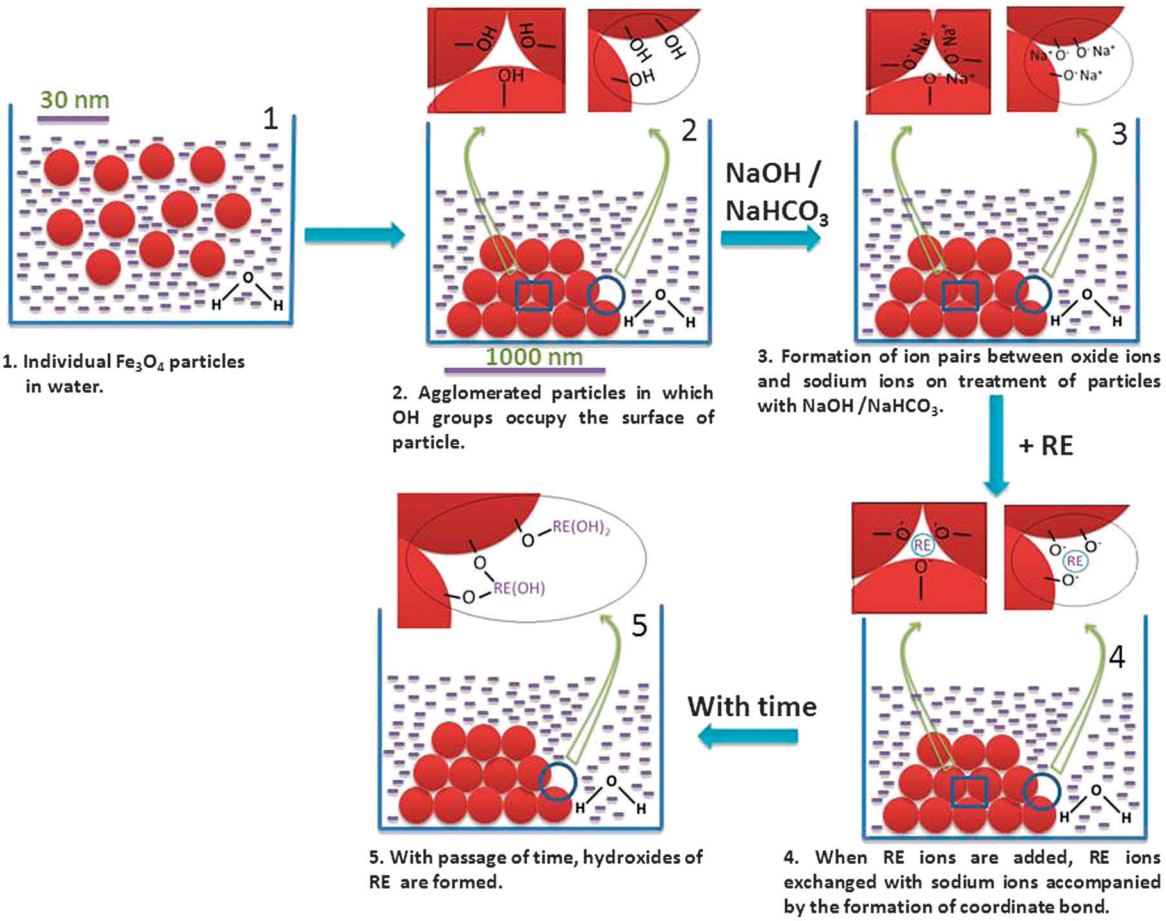

Fig. 1 Schematic diagram of the formation of agglomerated Fe_3O_4 particles and their sites where absorptions of radiolanthanide ions (indicated as 'RE') can take place.

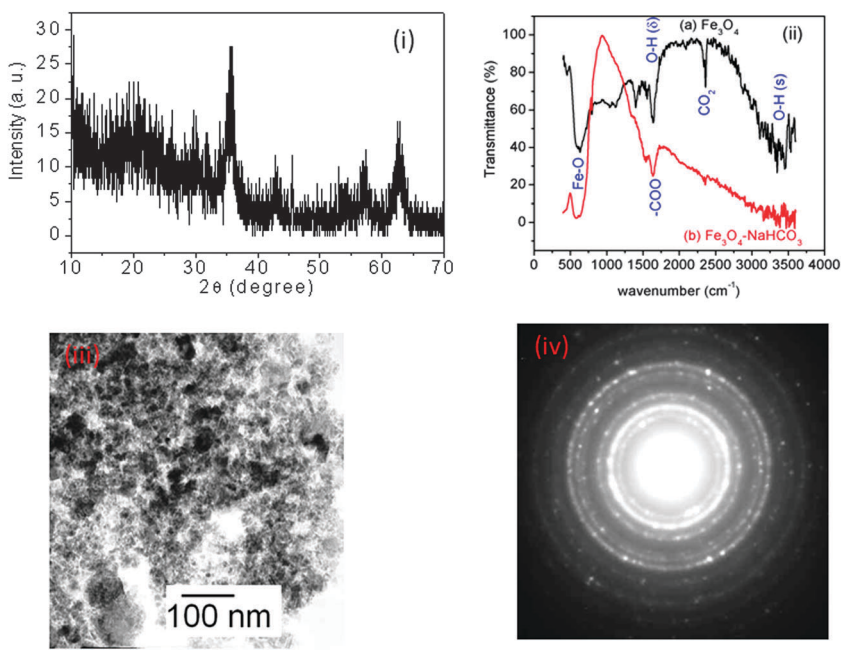

Fig. 2 (i) XRD pattern of Fe_3O_4 particles. (ii) FTIR spectra of Fe_3O_4 and Fe_3O_4 after treatment with a $NaHCO_3$ solution. (iii) TEM image of Fe_3O_4. (iv) SAED pattern of Fe_3O_4.

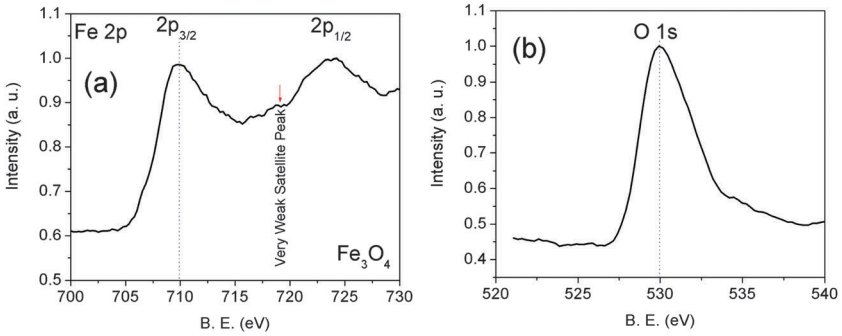

Fig. 3 XPS spectra of Fe 2p and O 1s in a Fe_3O_4 sample.

Table 2 Specific activity and radionuclide purities of radionuclides produced for loading on AgI-MNPs at 6 h post EOI

Radionuclide	Yield (GBq mg^{-1})	% Radionuclidic purity	Impurities detected
^{90}Y (reactor)	0.9 ± 0.06	99.93 ± 0.01	^{89}Sr, ^{91}Y, ^{169}Yb, ^{160}Tb
^{90}Y (generator)	NCA	>99.99	—
^{166}Ho	13.3 ± 0.4	99.99 ± 0.002	^{166m}Ho
^{153}Sm	44.4 ± 1.1	99.98 ± 0.005	^{154}Eu
^{177}Lu	931 ± 26	99.98 ± 0.005	^{177m}Lu
^{169}Er	0.4 ± 0.05	99.95 ± 0.01	^{169}Yb, ^{171}Tm

[a] Neutron irradiation at a thermal flux of 1×10^{14} n cm^{-2} s^{-1} for a duration of 7 d for Ho and Sm; 14 d for Y; 21 d for Lu and 28 d for Er. n = 3 for each radionuclide.

radionuclides vary widely from ^{169}Er (0.4 ± 0.05 GBq mg^{-1}) to ^{177}Lu (930.8 ± 25.6 GBq mg^{-1}).

Formulation of radiolanthanide-loaded agglomerated Fe_3O_4 nanoparticles

With an aim to arrive at the optimum conditions for formulation of radiolanthanide AgI-MNPs with maximum yield, a detailed study on the influence of various experimental parameters on the radiolabeling yield was carried out. All the optimization studies were carried out using ~185 MBq activity of ^{90}Y, ^{153}Sm, ^{166}Ho and ^{177}Lu; and ~37 MBq activity of ^{169}Er, which could be considered as the clinically relevant doses for treatment of arthritis for various joints.[10] The effect of variation of the concentration of AgI-MNP on the yield of each of the radiolanthanide loaded AgI-MNP is shown in Fig. 4. In all the cases reactions were carried out at pH ~ 8 for 30 min at room temperature. It was found that while NCA ^{90}Y-loaded AgI-MNP could be prepared in high yield of 96.4 ± 0.8% using 2 mg particles in 1 mL reaction volume, for other radionuclides including (n,γ) produced ^{90}Y, the minimum amount of particles required for obtaining >95% yield was 5 mg. Consequently, 5 mg mL^{-1} was considered as the optimum particulate concentration for formulation of clinically relevant doses of radiolanthanide loaded particulates. Variation of the pH of the reaction mixture between 2 and 10 showed that the pH did not have any significant effect on the yield within the range of 5–10. Below pH 5, the yields were found to be poor. The optimum pH for formulation of radiolanthanide loaded particulates was therefore considered to be ~7–8, which is advantageous as it

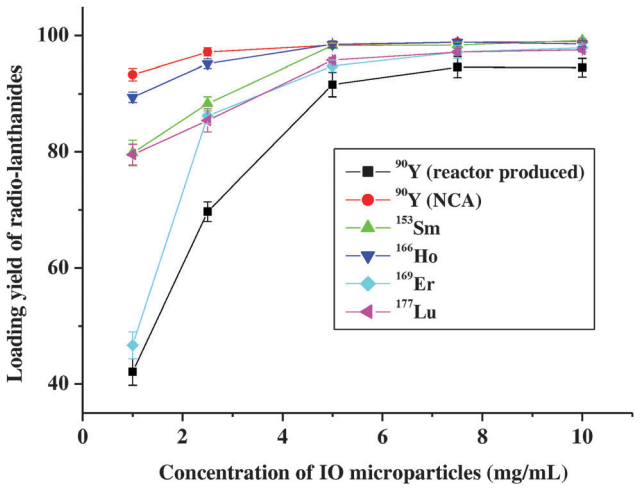

Fig. 4 The effect of variation of the concentration of AgI-MNP on the yield of radiolanthanide loaded particles.

is close to the physiological pH. Furthermore, it was found that when the reaction was carried out in 0.1 M $NaHCO_3$ medium, the pH was automatically adjusted within 7–8 when *MCl_3 (M = Y, Sm, Ho, Er and Lu) solution was added to the suspension of Fe_3O_4 particles. When loading yields were determined at different time points during the reaction, it was observed that the yield gradually increased with reaction time and reached maximum when the reactants were mixed for 30 min of incubation at room temperature.

Ion pair formation ($-O^-:Na^+$) helps in loading of Ln^{3+} ions over the particle. Ln^{3+} ion exchanges $3Na^+$ ions to form $-O^-:Ln^{3+}$ and then finally, hydroxylation takes place to form $-O^-$:RE–OH. The loading of RE ions over the surface of Fe_3O_3 is schematically shown in Fig. 1.

In vitro stability studies

Radiolanthanide-loaded AgI-MNPs showed excellent *in vitro* stability up to a study period of ~3 half-lives of respective lanthanide radionuclides when stored in normal saline at 37 °C. The radiochemical purities of all the preparations were found to be retained to the extent of >98% during the entire study period. In the DTPA challenge study, it was observed that the radiochemical purities of all the preparations under investigation gradually degraded in 5 mM DTPA solution as shown

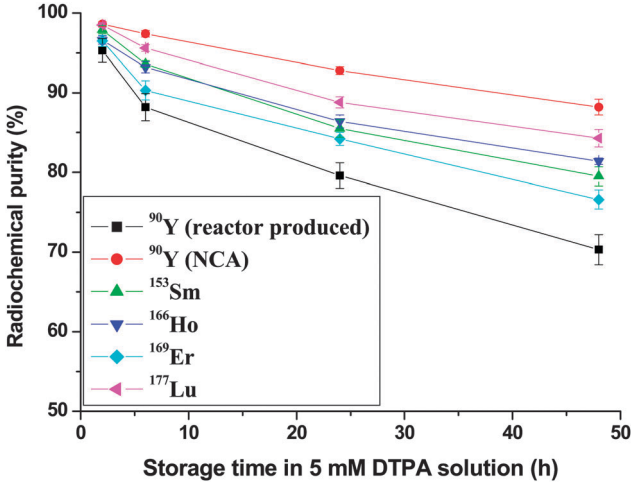

Fig. 5 Variation of radiochemical purities of radiolanthanide loaded Agl-MNPs with time when stored in 5 mM aqueous solution of DTPA at room temperature.

in Fig. 5. This gradual degradation is most likely due to leaching of lanthanide ions from the loaded particles and formation of the Ln–DTPA complex. However, it is pertinent to note that the radiochemical purities of the loaded particulates were found to be retained to the extent of >70% even after 48 h of storage, even when they were challenged by the strong chelator DTPA present at a concentration as high as 5 mM. This indicates fairly strong chemical association of lanthanides with particles, an essential prerequisite for designing radiotherapeutic agents for radiation synovectomy.

SEM and EDX analyses of Ho-loaded Fe_3O_4 particles

A typical scanning electron micrograph of holmium loaded Agl-MNP is shown in Fig. 6. The SEM result revealed that the particles have porous architecture throughout the matrix. The porous surface has an advantage because it can facilitate the diffusion of lanthanide for adsorption on the internal surface of the particulates. The micrograph also revealed that the size of holmium loaded particles ranged from 1–10 μm.

To verify the elemental composition and ensure the incorporation of Ho into the matrix, an EDX profile of holmium loaded particles has also been recorded as shown in Fig. 7. The EDX spectrum of Ho–Fe_3O_4 particles shows the presence of Fe, O and Ho confirming the incorporation of holmium into the particles. The chemical composition of the Ho–Fe_3O_4 surface was determined from the intensity of the peak pertaining to different elements and the quantification of results is given in Table 3.

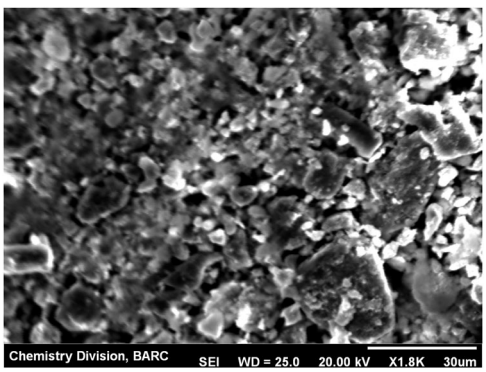

Fig. 6 A typical scanning electron micrograph of holmium loaded Agl-MNPs.

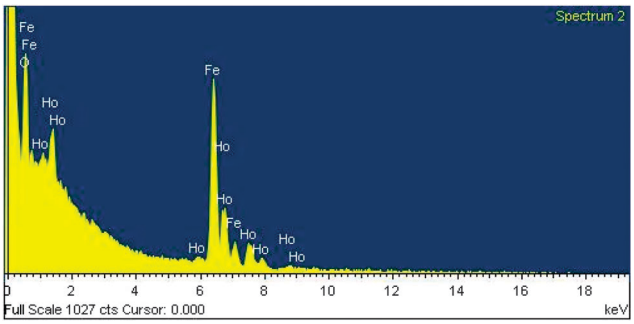

Fig. 7 EDX profile of holmium loaded Agl-MNPs.

Table 3 Chemical composition of the surface of Ho-loaded particles Fe_3O_4 as obtained from EDX analysis

Elements	Intensity corrn.	Weight (%)	Atom (%)
Oxygen	1.116	30.8 ± 1.4	69.44
Iron	0.964	36.1 ± 1.0	23.34
Holmium	0.918	33.1 ± 1.2	7.23

In vivo studies in an animal model

The results of the bio-distribution studies carried out in normal Wistar rats after loco-regional administration of ^{90}Y- and ^{166}Ho-loaded Agl-MNPs into one of the knee joint cavities of the animals are summarized in Tables 4 and 5, respectively. The results showed retention of >98% of the injected activity within the joint cavity even after 72 h p.i. for ^{90}Y- and 48 h for ^{166}Ho-loaded particles up to which studies were carried out. The activity detected in blood and other major organs/tissues was insignificant. The percentage of administered activity estimated to be excreted from the animals was also very low. These results indicated that there was almost no leakage of injected activity from the joint cavity of the animals.

The sequential whole-body radio-luminescence images of the Wistar rat acquired 30 min, 3 h, 24 h, and 72 h post-injection of ^{90}Y-loaded particles into one of the knee joints are shown in Fig. 8(a) to (d), respectively. Similarly, Fig. 9(a) to (d) show the images of animals administered with ^{166}Ho-loaded particles at 30 min, 3 h, 24 h, and 48 h post-injection. It is evident from these figures that almost all the injected activity remained localized in the synovium till the time post-administration up to which studies were carried out ($>T_{1/2}$ of ^{90}Y and $\sim 2T_{1/2}$ of ^{166}Ho). No activity could be detected in any other organ/tissue thereby confirming that practically no leakage of instilled particles had occurred. This observation has been corroborated with the results of the bio-distribution studies.

Table 4 Biodistribution pattern of ^{90}Y-loaded Fe_3O_4 particles administered in one of the knee joints of normal Wistar rats

	% Injected activity in organ/tissue		
Organ	3 h	24 h	72 h
Blood	0.01 (0.01)	0.01 (0.01)	0.00 (0.00)[a]
Liver	0.23 (0.05)	0.22 (0.06)	0.18 (0.03)
GIT	0.07 (0.02)	0.03 (0.01)	0.02 (0.01)
Kidney	0.02 (0.00)	0.01 (0.01)	0.00 (0.00)[a]
Stomach	0.00 (0.00)[a]	0.00 (0.00)[a]	0.00 (0.00)[a]
Heart	0.00 (0.00)[a]	0.00 (0.00)[a]	0.00 (0.00)[a]
Lungs	0.05 (0.03)	0.03 (0.02)	0.02 (0.02)
Skeleton	0.11 (0.04)	0.13 (0.03)	0.10 (0.04)
Muscle	0.00 (0.00)	0.00 (0.00)	0.00 (0.00)[a]
Spleen	0.04 (0.02)	0.04 (0.03)	0.03 (0.01)
Injected knee	**98.94 (0.28)**	**98.86 (0.34)**	**98.52 (0.29)**
Control knee	0.03 (0.01)	0.05 (0.02)	0.02 (0.02)
Excretion[b]	0.49 (0.15)	0.60 (0.18)	1.09 (0.22)

Values in the parentheses represent standard deviation.At every time point 4 animals have been used. ^{90}Y-Fe_3O_4 preparation was injected into the synovial cavity of the arthritis affected knee joints of each animal. [a] No detectable radioactivity above background. [b] Excretion has been calculated by subtracting the activity accounted in all the organs from the total activity injected.

Table 5 Bio-distribution pattern of ^{166}Ho-loaded Fe_3O_4 particles administered in one of the knee joints of normal Wistar rats

	% Injected activity in organ/tissue		
Organ	3 h	24 h	48 h
Blood	0.01 (0.01)	0.00 (0.00)[a]	0.00 (0.00)[a]
Liver	0.17 (0.06)	0.12 (0.05)	0.10 (0.03)
GIT	0.06 (0.02)	0.04 (0.02)	0.02 (0.01)
Kidney	0.03 (0.01)	0.02 (0.02)	0.00 (0.00)[a]
Stomach	0.00 (0.00)[a]	0.00 (0.00)[a]	0.00 (0.00)[a]
Heart	0.00 (0.00)[a]	0.00 (0.00)[a]	0.00 (0.00)[a]
Lungs	0.06 (0.03)	0.04 (0.01)	0.03 (0.01)
Skeleton	0.09 (0.03)	0.06 (0.03)	0.03 (0.03)
Muscle	0.00 (0.00)[a]	0.00 (0.00)[a]	0.00 (0.00)[a]
Spleen	0.04 (0.03)	0.04 (0.02)	0.03 (0.02)
Injected knee	99.01 (0.21)	98.82 (0.46)	98.88 (0.55)
Control knee	0.02 (0.02)	0.03 (0.02)	0.02 (0.01)
Excretion[b]	0.51 (0.12)	0.84 (0.26)	0.89 (0.16)

Values in the parentheses represent standard deviation.At every time point 4 animals have been used. ^{166}Ho-Fe_3O_4 preparation was injected into the synovial cavity of the arthritis affected knee joints of each animal. [a] No detectable radioactivity above background. [b] Excretion has been calculated by subtracting the activity accounted in all the organs from the total activity injected.

Discussion

The role of RSV as a safe, minimally invasive and cost effective therapeutic option in the management of different kinds of arthritis hardly needs to be reiterated.[43] The progress in this radiotherapeutic modality has been largely due to availability of more potent radioactive agents. The biological mechanism of RSV essentially involves the absorption of radioactive particulates by superficial cells of the synovium followed by phagocytosis by the macrophages of the inflamed synovium. Beta radiation causes coagulation necrosis, fibrosis and sclerosis of the proliferating synovial tissue and leads to destruction of the diseased pannus and inflamed synovium.[3,5,8,9] This prevents the secretion of fluid and accumulation of inflammation causing cellular compounds and the joint surfaces become fibrosed, offering rapid and sustained pain relief. The effective cytotoxic radiation dose required to be delivered to the joints is determined principally by the size of the joint along with other factors such as synovial thickness, synovial structures (smooth, villous-fine/rough edematous), condition of the

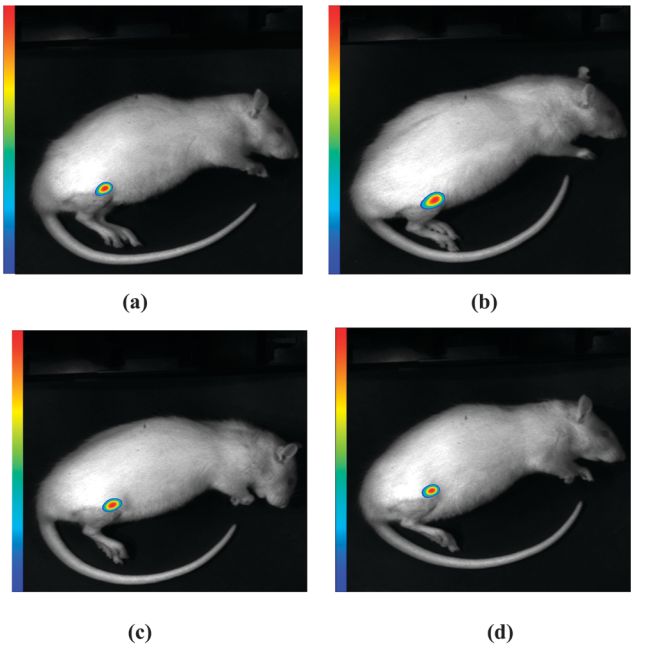

Fig. 8 Sequential whole-body radio-luminescence images of a normal Wistar rat acquired 30 min (a), 3 h (b), 24 h (c), and 72 h (d) post-injection of ^{90}Y-loaded AgI-MNP into one of the knee joints.

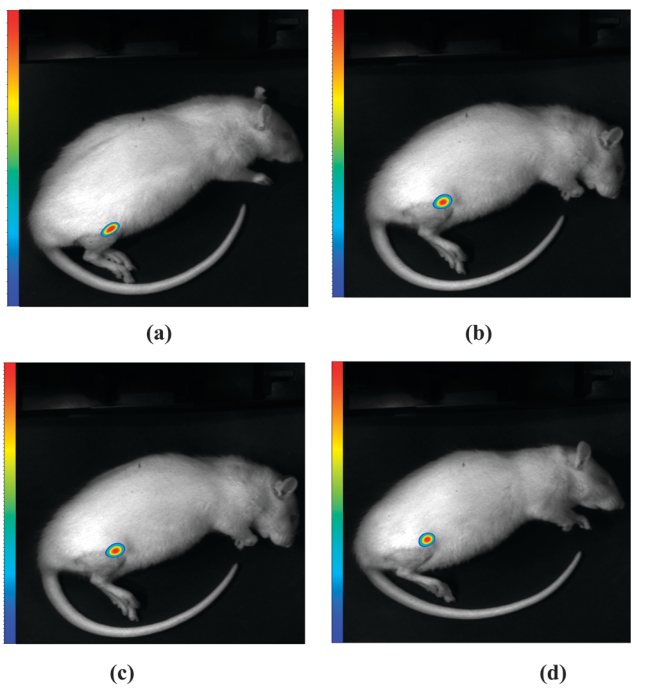

Fig. 9 Sequential whole-body radio-luminescence images of a normal Wistar rat acquired 30 min (a), 3 h (b), 24 h (c), and 48 h (d) post-injection of ^{166}Ho-loaded AgI-MNP into one of the knee joints.

joint fluid (watery or gelatinous) and inflammatory activity of the synovium.

The exciting perspective of radiolanthanides in RSV is primarily attributed to their ideally suited nuclear decay properties, favorable production logistics and availability of biocompatible materials where lanthanides can be irreversibly loaded. Table 1 shows a list of such radionuclides with their decay properties and the routes of their production. The selection of radiolanthanides for a specified application is primarily dictated by the physical half live, the mean tissue penetration range of the emitted β^- particles and the size of the joint to be treated. The penetration depth of the β^- radiation energy should correspond to the thickness of the synovium in the joint to be treated as inadequate penetration will have an inferior therapeutic effect, and excessive penetration would lead to radiation dose to healthy tissues. These factors have motivated the use of ^{90}Y, ^{166}Ho, ^{153}Sm, ^{177}Lu and ^{169}Er for this investigation.

The inherent success of RSV also resides on the selection an effective particulate carrier for the radionuclide. The particle used in RSV should be biocompatible, non-toxic, preferably biodegradable and have surface sites that allow absorption or binding of the radionuclide. The binding between the radionuclide and the particle should be essentially irreversible through the course of radiotherapy in order to prevent the leakage of radioactive material from the joint and to avoid whole-body radiation and its systemic effects. Our interest on the use of iron oxide nanoparticles spawned from their inimitable physicochemical characteristics including low toxicity, chemical inertness, biocompatibility, and possibility of surface functionalization for absorption/binding of metal ions.[27,30] Iron oxide nanoparticles are clinically approved metal oxide nanoparticles and have been shown to be associated with low toxicity in the human body.[44] Recent studies reported with supermagnetic iron oxide nanoparticles showed that the administered nanoparticles were gradually degraded form the organs and biotransformed into poorly magnetic iron species, which were believed to be stored into ferritin proteins over a period of three months.[45,46]

Owing to the large surface-to volume ratio, iron oxide nanoparticles possess high surface energies and thus tend to aggregate so as to minimize the surface energies. The agglomeration tendency offers the scope for preparing agglomerated Fe_3O_4 nanoparticles of 1–10 μm size range. While a number of strategies for radiolabeling of Fe_3O_4 nanoparticles have been reported, chelator free radiolabeling by noncovalent physisorption appeared to be enticing and the least intricate route.[34,38] This strategy has been successfully followed in the present work. Fe_3O_4 nanoparticles exhibit intrinsic surface reactivity and in aqueous solution coordinated with water to bear surface hydroxyl groups.[47] These reactive –OH groups upon subsequent dissociation generate ion pairs ($-O^-$:Na^+) when these particles are dispersed in a $NaHCO_3$ solution at pH = 7. The ion pair ($-O^-$:Na^+) formation on the nanostructured Fe_3O_4 scaffolds provides a versatile binding site and made it a viable strategy to attach or bind positively charged radiolanthanides by replacing Na^+ ions. Such a strategy constitutes an advantageous attribute in the endeavor of preparing radiolanthanide conjugates based on a single carrier platform.

In the last few decades, a large number of radiolabeled agents have been extensively studied in animal models and some in human patients for their use in RSV. Among these, a few agents namely, ^{90}Y-silicate/citrate colloid, ^{186}Re-sulfide colloid and ^{169}Er-citrate colloid have been approved for use in large, medium and small joints, respectively. All these approved agents are basically radiocolloids. However, one of the drawbacks associated with these agents is lack of control of particle size during their syntheses. This sometimes may lead to the leakage of the radioactivity from the diseased joints in case very small (nm dimension) radioactive particles are instilled. Any such leakage would result in accumulation of radioactivity in non-target organs such as liver, lung, spleen, *etc.* Contrary to this, in the case of the radiolanthanide loaded AgI-MNPs proposed in the present study the radionuclide is loaded onto the preformed particles of appropriate size. *In vitro* stability studies and *in vivo* biodistribution as well imaging studies in Wistar rats carried out using ^{90}Y- and ^{166}Ho-loaded particles clearly demonstrated that the synthesized radiolanthanide-loaded preparations are highly stable and there is almost no dislodging of radiolanthanides form the loaded particles *in vivo*. Based on these encouraging features together with the biocompatible nature of iron oxide nanoparticles, the developed formulations are presumed to have excellent therapeutic efficacy with minimal side effects.

Conclusions

The objective of development of a synthetic protocol based on a simple co-precipitation method that led to the formation of agglomerated Fe_3O_4 nanoparticles, with a size distribution (1–10 μm) optimal for use in RSV, has been successfully achieved. The surface chemistry of Fe_3O_4 nanoparticles has been utilized to achieve irreversible binding of radiolanthanide ($^*Ln^{3+}$) ions with the particle. Following the optimized procedure, it was possible to prepare radiolanthanide loaded particulates with >95% yields and >99% radiochemical purities. All the radioactive preparations exhibited very good *in vitro* stability. *In vivo* studies in animal models confirmed the near complete retention (>98% of administered radioactivity) of ^{90}Y- and ^{166}Ho-loaded particles into the knee joint cavities of normal Wistar rats even after 72 h post injection. These results amply indicate the potential utility of these agents for treatment in arthritic patients. The important details available from this investigation would be of considerable value and would stimulate researchers to pursue development of potent radioactive particles based on a nanoparticle platform for use in RSV.

Disclosure statement

The authors have neither received any outside funding nor any grants from any external agencies in support of this study. Our institutions do not have a financial relationship with any commercial entity that has an interest in the subject matter or materials discussed in this manuscript. None of the authors

in this manuscript have any conflict of interest, financial or otherwise in the publication of this material.

Acknowledgements

Research at the Bhabha Atomic Research Centre is part of the ongoing activities of the Department of Atomic Energy, India, and is fully supported by government funding. Authors wish to thank Dr K. L. Ramakumar, Director, Radiochemistry and Isotope Group, Dr B. N. Jagatap, Director, Chemistry Group and Dr V. K. Jain, Head, Chemistry Division of Bhabha Atomic Research Centre for their keen interest and providing necessary support during this study. The authors also gratefully acknowledge all the staff members of Isotope Production and Applications Division of Bhabha Atomic Research Centre associated with the production of the radionuclides used in the present investigation. KSS acknowledges UGC, Delhi, for providing JRF-NET fellowship.

References

1 J. R. O'Dell, in *Rheumatoid arthritis: the clinical picture, in arthritis and allied conditions: a textbook of rheumatology*, ed. W. J. Koopman, Lippincott Williams & Wilkins, Philadelphia, 14th edn, 2001, pp. 1153–1186.
2 M. Chinol, S. Vallabhajosula, S. J. Goldsmith, M. J. Klein, K. F. Deutsch, L. K. Chinen, J. W. Brodack, E. A. Deutsch, B. A. Watson and A. J. Tofe, *J. Nucl. Med.*, 1993, **34**, 1536–1542.
3 P. Schneider, J. Farahati and C. Reiners, *J. Nucl. Med.*, 2005, **46**, 48S–54S.
4 M. Fisher and G. Modder, *Nucl. Med. Commun.*, 2002, **23**, 829–831.
5 E. Deutsch, J. W. Brodack and K. F. Deutsch, *Eur. J. Nucl. Med.*, 1993, **20**, 1113–1127.
6 M. E. Siegel, H. J. Siegal and J. V. Luck, *Semin. Nucl. Med.*, 1997, **4**, 364–371.
7 S. Ofluoglu, E. Schwameis, H. Zehetgruber, E. Havlik, A. Wanivenhaus, I. Schweeger, K. Weiss, H. Sinzinger and C. Pirich, *J. Nucl. Med.*, 2002, **43**, 1489–1494.
8 G. Mödder, Radiation Synovectomy, in *Clinical Nuclear Medicine*, ed. H. J. Biersack and L. M. Freeman, Springer Verlag, Berlin Heidelberg, 2007, pp. 512–518.
9 S. J. Wang, W. Y. Lin, M. N. Chen, J. T. Chen, W. L. Ho, B. T. Hsieh, H. Huang, L. H. Shen, G. Ting and F. F. Knapp Jr., *Nucl. Med. Biol.*, 2001, **28**, 727–732.
10 G. Clunie and M. Fisher, *Eur. J. Nucl. Med. Mol. Imaging*, 2003, **30**, BP12–BP16.
11 F. M. Van Der Zant, R. O. Boer, J. D. Moolenburgh, Z. N. Jahangier, J. W. J. Bijlsma and J. W. G. Jacobs, *Clin. Exp. Rheumatol.*, 2009, **27**, 130–139.
12 M. Torres, E. Ayra, O. Albuerne and M. A. Montano Delgado, *Rev. Esp. Med. Nucl.*, 2009, **28**, 188–192.
13 W. U. Kampen, M. Voth, J. Pinkert and A. Krause, *Rheumatology*, 2007, **46**, 16–24.
14 P. R. Unni, P. R. Chaudhari, M. Venkatesh, N. Ramamoorthy and M. R. A. Pillai, *Nucl. Med. Biol.*, 2002, **29**, 199–209.
15 G. Clunie, D. Lui, I. Cullum, J. C. W. Edwards and P. J. Ell, *J. Nucl. Med.*, 1995, **36**, 51–57.
16 M. K. Bakht and M. Sadeghi, *Anal. Nucl. Med.*, 2011, **25**, 529–535.
17 S. Chakraborty, T. Das, S. Banerjee, S. Subramanian, H. D. Sarma and M. Venkatesh, *Nucl. Med. Biol.*, 2006, **33**, 585–591.
18 S. Chakraborty, T. Das, S. Banerjee, H. D. Sarma and M. Venkatesh, *Nucl. Med. Commun.*, 2006, **27**, 661–668.
19 S. Chakraborty, T. Das, V. Chiraiyal, S. P. Lohar and H. D. Sarma, *Radiochim. Acta*, 2014, **102**, 443–450.
20 A. Kahan, G. Mödder, C. J. Menkes, P. Verrier, J. Y. Devaux, A. Bonmartin, Y. De Rycke, L. Manil, F. Chossat and J. Tebib, *Clin. Exp. Rheumatol.*, 2004, **22**, 722–726.
21 S. Chakraborty, K. V. Vimalnath, A. Rajeswari, A. Shinto, H. D. Sarma, K. Kamaleshwaran, P. Thirumalaisamy and A. Dash, *J. Labelled Compd. Radiopharm.*, 2014, **57**, 453–462.
22 K. V. Vimalnath, S. Chakraborty, A. Rajeswari, H. D. Sarma, J. Nuwad, U. Pandey, K. Kamaeshwaran, A. Shinto and A. Dash, *Nucl. Med. Biol.*, 2015, **42**, 455–464.
23 U. Pandey, K. N. Bapat, G. Samuel, H. D. Sarma, P. R. Chaudhari, P. S. Dhami, R. Kannan and M. Venkatesh, *Nucl. Med. Commun.*, 2005, **26**, 459–463.
24 D. J. Hantowich, R. I. Kramer, C. B. Sledge, J. Noble and S. Shortkroff, *J. Nucl. Med.*, 1978, **19**, 303–308.
25 D. Peer, J. M. Karp, S. Hong, O. C. Farokhzad, R. Margalit and R. Langer, *Nat. Nanotechnol.*, 2007, **2**, 751–760.
26 M. Ferari, *Nat. Rev. Cancer*, 2005, **5**, 161–171.
27 S. Laurent, D. Forge, M. Port, A. Roch, C. Robic, L. Vander Elst and R. N. Muller, *Chem. Rev.*, 2008, **108**, 2064–2110.
28 M. K. Yu, Y. Y. Jeong, J. Park, S. Park, J. W. Kim, J. J. Min and S. Jon, *Angew. Chem., Int. Ed.*, 2008, **47**, 5362–5365.
29 X.-H. Peng, X. Qian, H. Mao, A. W. Wang, Z. Chen, S. Nie and D. M. Shin, *Int. J. Nanomed.*, 2008, **3**, 311–321.
30 R. Hao, R. Xing, Z. Xu, Y. Hou, S. Gao and S. Sun, *Adv. Mater.*, 2010, **22**, 2729–2742.
31 H. Y. Lee, Z. Li, K. Chen, A. R. Hsu, C. Xu, J. Xie, S. Sun and X. Chen, *J. Nucl. Med.*, 2008, **49**, 1371–1379.
32 R. Chakravarty, H. F. Valdovinos, F. Chen, C. M. Lewis, P. Ellison, H. Luo, E. Meyerand, R. J. Nickles and W. Cai, *Adv. Mater.*, 2014, **26**, 5119–5123.
33 A. C. Silva, T. R. Oliveira, J. B. Mamani, S. M. F. Malheiros, L. Malavolta, L. F. Pavon, T. T. Sibov, E. Amaro Jr., A. Tannús, E. L. G. Vidoto, M. J. Martins, R. S. Santos and L. F. Gamarra, *Int. J. Nanomed.*, 2011, **6**, 591–603.
34 M. M. Paulides, J. F. Bakker, A. P. M. Zwamborn and G. C. van Rhoon, *Int. J. Hyperthermia*, 2007, **23**, 59–67.
35 P. K. Sneed, P. R. Stauffer, M. W. McDermott, C. J. Diederich, K. R. Lamborn, M. D. Prados, S. Chang, K. A. Weaver, L. Spry, M. K. Malec, S. A. Lamb, B. Voss, R. L. Davis, W. M. Wara, D. A. Larson, T. L. Phillips and P. H. Gutin, *Int. J. Radiat. Oncol., Biol., Phys.*, 1998, **40**, 287–295.
36 E. Boros, A. M. Bowen, L. Josephson, N. Vasdev and J. P. Holland, *Chem. Sci.*, 2015, **6**, 225–236.
37 R. Chakravarty, U. Pandey, R. B. Manolkar, A. Dash, M. Venkatesh and M. R. A. Pillai, *Nucl. Med. Biol.*, 2008, **35**, 245–253.

38 U. Pandey, P. S. Dhami, P. Jagesia, M. Venkatesh and M. R. A. Pillai, *Anal. Chem.*, 2008, **80**, 801–807.
39 A. Ruggiero, J. P. Holland, J. S. Lewis and J. Grimm, *J. Nucl. Med.*, 2010, **51**, 1123–1130.
40 R. Ghosh, L. Pradhan, Y. P. Devi, S. S. Meena, R. Tewari, A. Kumar, S. Sharma, N. S. Gajbhiye, R. K. Vatsa, B. N. Pandey and R. N. Ningthoujam, *J. Mater. Chem.*, 2011, **21**, 13388–13398.
41 A. I. Prasad, A. K. Parchur, R. R. Juluri, N. Jadhav, B. N. Pandey, R. S. Ningthoujam and R. K. Vatsa, *Dalton Trans.*, 2013, **42**, 4885–4896.
42 T. Fujii, F. M. F. de Groot, G. A. Sawatzky, F. C. Voogt, T. Hibma and K. Okada, *Phys. Rev. B: Condens. Matter Mater. Phys.*, 1999, **59**, 3195–3202.
43 M. E. Siegel, H. J. Siegel and J. V. Luck Jr., *Semin. Nucl. Med.*, 1997, **27**, 364–371.
44 N. Singh, G. J. S. Genkins, R. Asadi and S. H. Doak, *Nano Rev.*, 2010, **1**, 5358, DOI: 10.3402/nano.v1i0.5358.
45 H. Chen, J. Burnett, F. Zhang, J. Zhang, H. Paholak and D. Sun, *J. Mater. Chem. B*, 2014, **2**, 757–765.
46 M. Levy, N. Luciani, D. Alloyeau, D. Elgrabli, V. Deveaux, C. Pechoux, S. Chat, G. Wang, N. Vats, F. Gendron, C. Factor, S. Lotersztajn, A. Luciani, C. Wilhelm and F. Gazeau, *Biomaterials*, 2011, **32**, 3988–3999.
47 K. Turcheniuk, A. V. Tarasevych, V. P. Kukhar, R. Boukherroub and S. Szunerits, *Nanoscale*, 2013, **5**, 10729–10752.

